8th ECCOMAS Thematic Conference on the Mechanical Response of Composites
COMPOSITES 2021
M. Fagerström & C. Catalanotti (Editors)

EVALUATION OF THE INFLUENCE OF THE MATRIX-INCLUSION INTERFACE BASED ON FFT METHODS

T.A Do[1⋆], P. Karamian-Surville[1⋆⋆]

[1] Normandie Univ, UNICAEN, CNRS, LMNO, 14000 Caen, France

⋆ tuan-anh.do@unicaen.fr

⋆⋆ philippe.karamian@unicaen.fr

Keywords: Homogenozation, Multiscale, FFT, Interphase, Composite.

Summary: *In order to take into account the effects of the interface between matrix and inclusion, an interphase is generated. A numerical homogenization process is then considered, based on multiscale technique for estimating the effective properties of composite materials by integrating the Lippmann-Schwinger equation. The algorithm is based on fast Fourier transform (FFT). However, considering an interphase brings up problems for FFT. As the interphase is very thin and due to inhomogeneities, the kernel (Green-kernel) must be also modified to get more accuracy in calculation. This approach is especially suitable for high and low contrasts, since that the number of voxels/pixels representing the same material is limited. This limit reduces the accuracy of FFT. In this framework, the paper studies different approaches to overcome the interphase problem. The effective material properties are estimated by using multilayer interphase as well as equivalent interphase in the homogenization procedure.*

1. INTRODUCTION

Composite materials are present at almost every level of the industry. These materials have a huge advantage due to a wide range of mechanical, thermal and electrical properties. Composite materials also have higher strength and modulus-to-weight ratios than traditional engineered materials. Since the discovery of carbon nanotubes more than thirty years ago by Iijima [1], there has been a great interest in nanocomposite technology. Compared to traditional composites, nanocomposites offer improved quality due to better contact between the matrix and the inclusion. Much research has proven this ability of nanomaterials and nanometric structure. [2, 3, 4, 5]

In terms of nanocomposite investigation, the scientists have worked on their properties through theoretical analyses, numerical computations, experimental studies and most recently artificial neural network. In [6], Cuenot et al. have measured the elastic properties of silver nanowires of 20 to 140 nm outer diameter. In [7], Blivi et al. have investigated the influence of particle size from 15nm to 500nm on mechanical and thermal properties. In [8], Chen et al. have developed an analytical model calculating the elastic modulus of SiC nanoparticle reinforced with the consideration of the size factor and aggregated state of the nanoparticles. In [9], Karimzadeh et al. have studied the ability of the nano-indentation method in the mechanical characterization of dental restorative nanocomposite (particle size from 50nm to 5 μm)

using experimental and finite elements approaches. In [10], Lee et al. have proposed new approach determining the nanomechanical stress-strain parameters using the indentation force-displacement relationship. This approach is based on the dimensional analysis and the Bayesian regularization training algorithm of the artificial neural networks.

To calculate the properties of composite materials, researchers have employed numerical methods such as molecular dynamics [11], finite elements method (FEM) [12], boundary element method (BEM) [13], methods based of FFT[14]. In the framework of FFT-based method a numerical process based on multiscale technique to estimate the effective properties by integrating the Lippmann-Schwinger equation is considered. This approach has several advantages: this method does not need to solve a linear system, time computation is reduced compared to other methods, SEM (Scanning Electron Microscopy) images can be used directly to analyze composite materials [15]. The FFT-based method can also deal with nonlinear behavior [16]. In [17], Lee et al. have used FFT algorithm to compute viscoplastic response under uniaxial tension of metal-metal composite. Recently, many scientists have worked on improving FFT algorithm, for instance, in [18], Monchiet et al. have proposed an iterative scheme based on polarization field to improve the convergence of FFT for composite with voids or rigid inclusions. In [19], Willot has presented a modified Green operator for thermal and elastic cases with higher convergence rates and more accuracy in calculation. In [20], Nguyen et al. have described a new Green operator for computing the effective elastic properties of periodic thin plates.

For the modeling of the heterogeneities, it is necessary to adopt a stochastic approach considering spatial position, the orientation and the morphology of the heterogeneities as random variables following probability laws to design NSREVs (Numerical Stochastic Representative Element Volume) [21, 22]. In addition to take into account the random aspect in the multiscale homogenization method, the interface effect must also be considered in the continuum mechanics modeling of nanomaterials and nanostructures. This area is different because of the high interface to volume ratio of materials, then one can consider the interface energy is comparable to bulk energy. To model this effect, researchers consider the different properties in the interaction zone via an interface or interphase. In [23], Miller et al. have used direct atomistic simulations of nanosized structures. In [24, 25], analytical models have been introduced considering interphase layer to evaluate elastic properties of nanocomposites. In [26], Duan et al. have proposed new frameworks to compute effective moduli of nanostructure taking into account surface stress effect based on Mori Tanaka method and the generalized self-consistent method. In [27], Dormieux et al. have introduced an equivalent inclusion combining the nanoparticle and surrounding interface. This approach can be directly implemented in Mori-Tanaka model. In [28], Yvonnet et al. have used the extended finite element method with the coherence interface model to investigate the size-dependent effective properties of nanocomposites.

This article deals with the consideration of the interface effect within the framework of the FFT-based methods for the integration of the Lippmann-Schwinger equation. We consider an interphase representing the contact between matrix and inclusions. In section 2. we briefly present the basics of FFT-based methods. The accelerated scheme [29] has been implemented

to deal with the high contrast case. To obtain more precision in the calculation and for any type of contrast, we have also implemented the modified Green operator proposed by Willot [19]. The following section shows the efficiency of the model with a simple example. Using this approach, we evaluate the effective properties of REV (Reprentative Volume Element) containing only matrix with inclusion (perfect bonding). The results are compared with the analytical method and FEM. In section 4, we consider the interface effect using this FFT-based method. First, a multi-layered approach has been introduced. Then, we propose an equivalent interphase replacing the multilayer. This approach is more efficient for FFT-based methods. The size effect is also discussed.

2. GENERAL FORMULATIONS

2.1 FFT based method

2.1.1 Cell problem

We consider an RVE (Representative Volume Element) V. The RVE can be represented by an image containing $N \times N \times N$ voxels. We consider the so-called cell problem with periodic boundary conditions. The local strain field $\varepsilon(\boldsymbol{u}(\boldsymbol{x}))$ is formed by a periodic part $\varepsilon(\boldsymbol{u}^{per}(\boldsymbol{x}))$ and an average strain $\boldsymbol{E}$:

$$\varepsilon(\boldsymbol{u}(\boldsymbol{x})) = \varepsilon(\boldsymbol{u}^{per}(\boldsymbol{x})) + \boldsymbol{E} \tag{1}$$

where $\boldsymbol{u}, \boldsymbol{u}^{per}, \boldsymbol{x}$ represent respectively the displacement, periodic displacement, local position respectively satisfying the zero mean on RVE: $< \varepsilon(\boldsymbol{u}^{per}(\boldsymbol{x})) >_V = 0$. Which is equivalent to:

$$\boldsymbol{u}(\boldsymbol{x}) = \boldsymbol{u}^{per}(\boldsymbol{x}) + \boldsymbol{E}\boldsymbol{x} \tag{2}$$

The local problem reads:

$$\left.\begin{aligned} \boldsymbol{\sigma}(\boldsymbol{x}) = \mathbb{C}(\boldsymbol{x})\varepsilon(\boldsymbol{u}(\boldsymbol{x})) = \mathbb{C}(\boldsymbol{x})(\varepsilon(\boldsymbol{u}^{per}(\boldsymbol{x})) + \boldsymbol{E}) \qquad \forall \boldsymbol{x} \in V \\ \mathbf{div}\boldsymbol{\sigma}(\boldsymbol{x}) = 0 \qquad \forall \boldsymbol{x} \in V, \boldsymbol{u}^{per} \text{periodic} \end{aligned}\right\} \tag{3}$$

where $\mathbb{C}(\boldsymbol{x})$ is the local stiffness tensor. Introducing a reference stiffness tensor $\mathbb{C}^0$ and a polarization field $\boldsymbol{\tau}(\boldsymbol{x}) = (\mathbb{C}(\boldsymbol{x}) - \mathbb{C}^0)\varepsilon(\boldsymbol{u}(\boldsymbol{x})) = \delta\mathbb{C}(\boldsymbol{x})\varepsilon(\boldsymbol{u}(\boldsymbol{x}))$. The equation 3 reads:

$$\left.\begin{aligned} \boldsymbol{\sigma}(\boldsymbol{x}) = \mathbb{C}^0(\varepsilon(\boldsymbol{u}(\boldsymbol{x}))) + \boldsymbol{\tau}(\boldsymbol{x}) \qquad \forall \boldsymbol{x} \in V \\ \mathbf{div}\boldsymbol{\sigma}(\boldsymbol{x}) = 0 \qquad \forall \boldsymbol{x} \in V \end{aligned}\right\} \tag{4}$$

Due to the equation satisfied by the polarization field. The interested reader can refer for example to ([30], p.251). Let us introduce periodic Green operator $\boldsymbol{\Gamma}^0$ associated with $\mathbb{C}^0$ then one can write:

$$\boldsymbol{\varepsilon}(\boldsymbol{u}(\boldsymbol{x})) = -\boldsymbol{\Gamma}^0 * \boldsymbol{\tau}(\boldsymbol{x}) + \boldsymbol{E} \qquad \forall \boldsymbol{x} \in V \tag{5}$$

Where * is the convolution product. In Fourier space the previous equation also reads :

$$\left.\begin{aligned} \hat{\boldsymbol{\varepsilon}}(\boldsymbol{\xi}) = -\hat{\boldsymbol{\Gamma}}^0(\boldsymbol{\xi}) : \hat{\boldsymbol{\tau}}(\boldsymbol{\xi}) \qquad & \forall \boldsymbol{\xi} \neq 0 \\ & \hat{\boldsymbol{\varepsilon}}(0) = \boldsymbol{E} \end{aligned}\right\} \tag{6}$$

2.1.2 Algorithm based on FFT

Algorithm 1: Acceleration scheme in elastic

Result: $\varepsilon(\boldsymbol{x})$
initialization: $\boldsymbol{\varepsilon}^0(\boldsymbol{x}) = \boldsymbol{E}, \epsilon_{comp} = 1., \epsilon_{eq} = 1., acc = 1e^{-6}$;
while $\epsilon_{comp} > acc \ \ \& \ \ \epsilon_{eq} > acc$ **do**
  Compute: $\boldsymbol{\sigma}(\boldsymbol{x}) = \mathbb{C}(\boldsymbol{x})\boldsymbol{\varepsilon}(\boldsymbol{x})$;
  if $\epsilon_{comp} < acc$ **then**
    $\hat{\boldsymbol{\sigma}}(\boldsymbol{\xi}) = FFT(\boldsymbol{\sigma}(\boldsymbol{x}))$;
    Compute ϵ_{eq};
  else
    $\epsilon_{eq} = 1.$;
  end
  $\boldsymbol{\tau}(\boldsymbol{x}) = (\mathbb{C}(\boldsymbol{x}) - \mathbb{C}^0)\boldsymbol{\varepsilon}(\boldsymbol{x})$;
  $\hat{\boldsymbol{\tau}}(\boldsymbol{\xi}) = FFT(\boldsymbol{\tau}(\boldsymbol{x}))$;
  $\hat{\boldsymbol{\varepsilon}}(\boldsymbol{\xi}) = -\hat{\boldsymbol{\Gamma}}^0(\boldsymbol{\xi}) : \hat{\boldsymbol{\tau}}(\boldsymbol{\xi})$;
  $\hat{\boldsymbol{\varepsilon}}(0) = \boldsymbol{E}$;
  $\boldsymbol{\varepsilon}_{comp}(\boldsymbol{x}) = FFT^{-1}(\hat{\boldsymbol{\varepsilon}}(\boldsymbol{\xi}))$;
  $\epsilon_{comp} = \frac{\sqrt{<||\boldsymbol{\varepsilon}(\boldsymbol{x}) - \boldsymbol{\varepsilon}_{comp}(\boldsymbol{x})||^2>}}{||\boldsymbol{E}||}$;
  $\boldsymbol{\varepsilon}(\boldsymbol{x}) = \boldsymbol{\varepsilon}(\boldsymbol{x}) - 2(\mathbb{C}(\boldsymbol{x}) + \mathbb{C}^0)^{-1}\mathbb{C}^0(\boldsymbol{\varepsilon}_{comp}(\boldsymbol{x}) - \boldsymbol{\varepsilon}(\boldsymbol{x}))$;
end

where the error ϵ_{eq} can be determined by:

$$\epsilon_{eq} = \frac{\sqrt{< ||\mathbf{div}\boldsymbol{\sigma}||^2 >}}{|| < \boldsymbol{\sigma} > ||} = \frac{\sqrt{< ||\boldsymbol{\xi}.\hat{\boldsymbol{\sigma}}(\boldsymbol{\xi})||^2 >}}{||\hat{\boldsymbol{\sigma}}(\mathbf{0})||} \tag{7}$$

2.2 Discrete algorithm

2.2.1 Traditional method

We discretize the unit cell into a grid of $N_1 \times N_2$ pixels in 2D and $N_1 \times N_2 \times N_3$ voxels in 3D. The data and the unknowns are stored in each pixel/voxel on this grid. For instance in 2D, the coordinates of the pixel (i_1, i_2) are:

$$\boldsymbol{x}(i_1, i_2) = (\frac{i_1 - 1}{N_1}, \frac{i_2 - 1}{N_2}), \qquad i_1 = 1, ..., N_1 \qquad i_2 = 1, ..., N_2$$

In the Fourier space, the discrete frequencies are:

$$\xi_j = 0, 1, 2, ..., \frac{N_j}{2}, (-\frac{N_j}{2} + 1), (-\frac{N_j}{2} + 2), ..., -2, -1$$

2.2.2 Modified Green operator

In this study, the modified Green operator [19] has been used. So, the strain field is defined on Fourier space as follows:

$$\varepsilon_{ij}(\boldsymbol{\xi}) = \frac{1}{2}[k_i(\boldsymbol{\xi})u_j(\boldsymbol{\xi}) + k_j(\boldsymbol{\xi})u_i(\boldsymbol{\xi})] \tag{8}$$

where $\boldsymbol{k}$ represents discrete gradient operator.

$$k_i(\boldsymbol{\xi}) = \frac{i}{4}\tan(\pi\xi_i)(1 + e^{2\pi i\xi_1})(1 + e^{2\pi i\xi_2})(1 + e^{2\pi i\xi_3}) \tag{9}$$

The Green operator becomes:

$$G_{ijkl}(\boldsymbol{\xi}) = \frac{(\lambda^0 + 2\mu^0)(r_i r_l^* \delta_{jk})_{sym} + \lambda^0[(r_i r_l^* \delta_{jk})_{sym} - \mathrm{Re}(r_i r_j^*)\,\mathrm{Re}(r_k r_l^*)] - \mu^0 r_i r_j r_k^* r_l^*}{\mu^0[2(\lambda^0 + \mu^0) - \lambda^0[|r_1^2 + r_2^2 + r_3^2|^2]} \tag{10}$$

where $r_i = k_i/|\boldsymbol{k}|$ and $\boldsymbol{s}$ is the symmetric second-order tensor:

$$s_{jj} = 4\,\mathrm{Im}(r_i r_k^*)^2, \qquad s_{jk} = -4\,\mathrm{Im}(r_k r_j^*)\,\mathrm{Im}(r_j r_k^*), \qquad i \neq j \neq k \tag{11}$$

with a^* is the complex conjugate of a, Re, Im are respectively real part, imaginary part of the enclosed complex quantity.

3. VALIDATION

First, in order to validate our approach, we compare the model with the analytical Mori-Tanaka method [31]. In figure 1a, we consider a spherical void inclusion, which means that $c = 0$, where c is the contrast. Three resolutions are taken into account: $128 \times 128 \times 128$, $256 \times 256 \times 256$ and $512 \times 512 \times 512$. In this example, we compute the effective bulk modulus of porous aluminum. The material parameters of the matrix are $E = 70$ MPa and $\nu = 0.32$. The estimation of effective properties has been provided by FEM [5, 28]. A perfect binding between the matrix and the inclusion is assumed. The reference normalized effective bulk modulus k^{eff}/k_M is computed, k_M is the matrix bulk modulus. For the matrix the parameters are set up to $k_M = 1$ and $\mu_M = 0.4$.

Figure 1 depicts the results for effective bulk modulus and the error of new approach for different resolutions and volume fraction. Compare to the classical Green-kernel , the modified

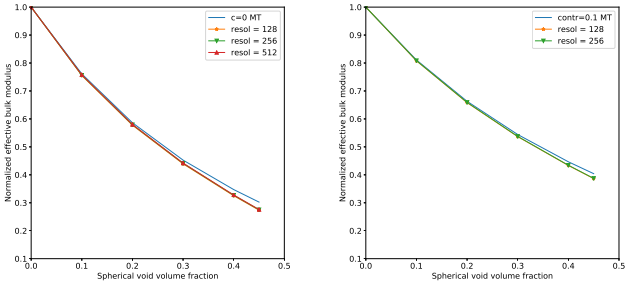

(a) Void inclusion (b) Constrast = 0.1

Figure 1. Normalized effective bulk modulus as function of volume fraction

Green-kernel approach converges more quickly. We observe a good agreement with analytical results no matter the resolution. For a contrast $c = 0.1$, higher value of effective bulk modulus is obtained. For example, at $f = 0.1$ the normalized effective modulus $k_{eff} = 0.74$ for void inclusion and $k_{eff} = 0.8$ for $c = 0.1$. The higher the resolution is, the more accurate results are obtained. In the next section, using the modified Green operator, we investigate the influence of interface effect to the performance of composite.

4. INTERFACE EFFECT

4.1 Multilayer

4.1.1 Modeling

Considering the interphase between the matrix and the inclusion, the material properties change following exponential rule [32, 33, 25] as shown in the figure 2. So, for an isotropic medium, the bulk modulus of interphase can be determined by the following relation:

$$k(r) = k_m(1 + (c - 1)(1 - re^{1-r})) \tag{12}$$

where r is the variable. $r = 0$ is the inclusion; $r = 1$ is the matrix.

4.1.2 Analytic result and FFT

First, the cylindrical inclusion model is dealt. To Describe the variation of elastic properties in the interphase, the interphase has been discretized in N layers. Within each layers, as illustrated in figure 2b, the elastic properties k_n, μ_n are proposed to be constant. These properties are determined by the equation 12. For two adjacent layers, a perfect binding assumption has been made. The contrast $c = 0.01$ is examined; this configuration gives a good rate of convergence, moreover, for $c = 0.01$ the gap between the properties of the matrix and the inclusion is large enough, so that we can observe the influence of the interface. Different numbers of layer have been evaluated from $N = 1 \rightarrow 8$. The numerical calculation is compared with the Mori-Tanaka

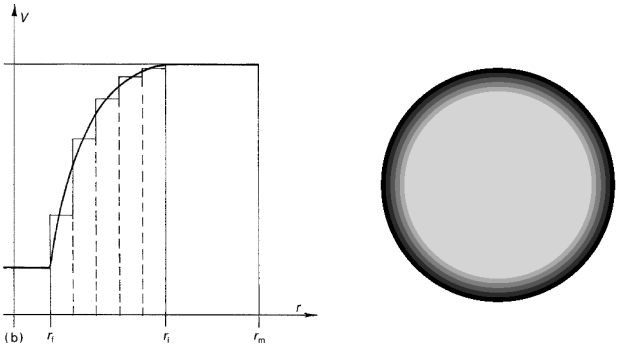

(a) Exponential rule (b) Discretization within the interphase

Figure 2. Variations of bulk modulus within the interphase and the discretization method. The error is determined as follows:

$$Error = \frac{|k^{FFT} - k^{MT}|}{k^{MT}} \tag{13}$$

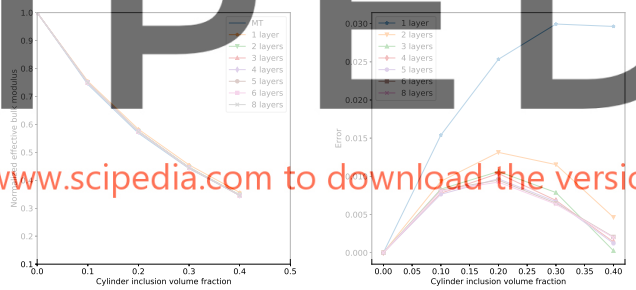

(a) Normalized effective bulk modulus (b) Error of normalized effective bulk modulus

Figure 3. MT vs Multilayer FFT

Figure 3 exhibits the results of effective bulk modulus and the error of FFT taking Mori-Tanaka as reference. We observe a very good agreement of FFT method for $N > 2$. The maximum error is less than 1.5 %

4.2 Equivalent interphase

It is more convenient to represent the interphase by one homogeneous layer. From the equation 12, we describe the equivalent elastic properties of the interphase by following equation:

$$k_{eq} = \int k(r)dr \tag{14}$$

From the configuration of previous example, with $c = 0.01$, $k_M = 1$ we get $k_{eq} = 0.7211$. The calculation is performed as in the case of three phase material. The result is compared to the previous Mori-Tanaka result.

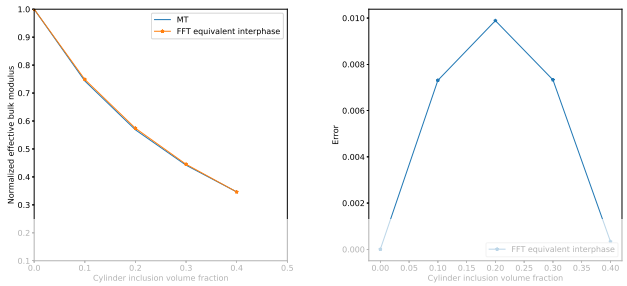

(a) Normalized effective bulk modulus (b) Error of normalized effective bulk modulus

Figure 4. MT vs Equivalent interphase FFT

Figure 4 shows the results of estimated effective bulk modulus and the error of equivalent model. We observe a very good agreement between the reference and the numerical calculation. The error is always less than 1.5 %.

4.3 Equivalent interphase model vs interface model

4.3.1 Spherical void

In this example, we consider the case of spherical void in 3D. This case has been investigated by FEM [28] and molecular dynamic [23]. The material parameters of the matrix are $E = 70$ MPa and $\nu = 0.32$. The surface parameter obtained through the molecular dynamics: $\lambda_s = 6.842$ N/m, $\mu_s = -0.375$ N/m. So the surface bulk modulus $k'_s = \lambda_s + 2\mu_s = 6.091$ N/m. At this configuration, the equivalent elastic properties of interphase is determined by:

$$k_{eq} = \frac{k'_s}{tk_M} \tag{15}$$

where t is the thickness of the interphase. First, we have arbitrarily chosen $t = 0.1R$. The result of the FFT is validated with the analytical approach[26]. This analytical approach is dedicated to spherical voids with a coherent surface.

Figure 5 shows the result of effective bulk modulus and the error of equivalent model for several resolutions. The model describes expected effect of interface between matrix and inclusion no matter the resolution . The results are in a good agreement with reference solutions when $f < 0.3$. The gap when $f > 0.3$ is due to the infinite contrast and the shape of REV as explained in [16].

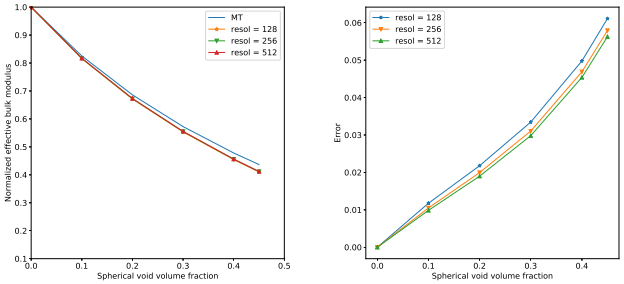

(a) Normalized effective bulk modulus (b) Error of normalized effective bulk modulus

Figure 5. MT interface model vs Equivalent FFT

4.4 Size effect

We can also use this approach for a size dependent problem. Two examples have been considered. For a constant volume fraction $f = 0.2$, we vary the radius of void and calculate for each size the effective volume modulus. The material properties are the same as in section 3 for the cylindrical inclusion in figure 6a. In figure 6b, the contrast is fixed to $c = 0.1$.

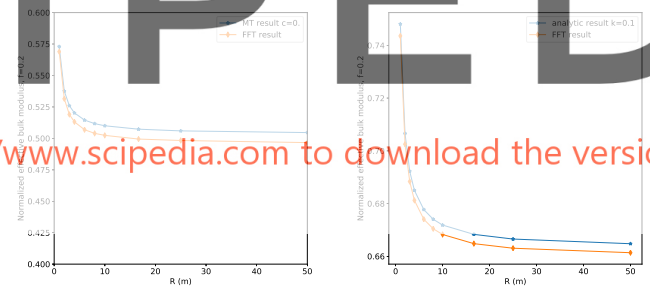

(a) cylinder (b) spherical

Figure 6. Size dependence

The figure 6 shows the expected size effect as presented in [28]. The effective properties depend clearly on nanovoid radius for small sizes of nanovoids, but these values are not sensitive to the radius for large sizes. A good agreement between the reference solution and the FFT-based method is observed. Indeed, the maximum or relative error is less than 1.6%.

5. CONCLUSIONS

In this work, the interface effect has been studied by the method based on the FFT. In order to reduce the computation time and obtain more precise results, within the framework of the FFT approach, the accelerated scheme with modified Green operator has been implemented. First, the new approach was validated for a perfect binding case. Next, we have considered an

interphase representation to study the interface effect. For the multi-layered approach, good agreement was obtained for the appropriate number layers. To reduce the complexity of the problem, we have also considered the equivalent interphase. We have compared the results with the analytical approach and FEM. The equivalent approach has proven to be efficient and reliable. Note that this approach can also be extended to plasticity. It remains to apply the present method to the case of the volume of stochastic representative element.

References

[1] Iijima, S. *Helical microtubules of graphitic carbon*. Nature **354**, 56–58 (1991).

[2] Sharma, P., and Ganti, S. (November 9, 2004). "Size-Dependent Eshelby's Tensor for Embedded Nano-Inclusions Incorporating Surface/Interface Energies ." ASME. *J. Appl. Mech.* September 2004; 71(5): 663–671. https://doi.org/10.1115/1.1781177

[3] Downing, T. D., et al. "Determining the interphase thickness and properties in polymer matrix composites using phase imaging atomic force microscopy and nanoindentation." *Journal of adhesion science and technology* 14.14 (2000): 1801-1812.

[4] Martinez-Ayuso, German, et al. "Homogenization of porous piezoelectric materials." *International Journal of solids and Structures* 113 (2017): 218-229.

[5] Bach, Dang Phong, Delphine Brancherie, and Ludovic Cauvin. "Size effect in nanocomposites: XFEM/level set approach and interface element approach." *Finite Elements in Analysis and Design* 165 (2019): 41-51.

[6] Cuenot, Stéphane, et al. "Surface tension effect on the mechanical properties of nanomaterials measured by atomic force microscopy." *Physical Review* B 69.16 (2004): 165410.

[7] A.S. Blivi, F. Benhui, J. Bai, D. Kondo, F. Bédoui, Experimental evidence of size effect in nano-reinforced polymers: Case of silica reinforced PMMA, *Polymer Testing* (2016), doi: 10.1016/j.polymertesting.2016.10.025.

[8] Chen, Shenggui, M. K. Hassanzadeh-Aghdam, and R. Ansari. "An analytical model for elastic modulus calculation of SiC whisker-reinforced hybrid metal matrix nanocomposite containing SiC nanoparticles." *Journal of Alloys and Compounds* 767 (2018): 632-641.

[9] Karimzadeh, A., R. Koloor, S.S., Ayatollahi, M.R. et al. Assessment of Nano-Indentation Method in Mechanical Characterization of Heterogeneous Nanocomposite Materials Using Experimental and Computational Approaches. *Sci Rep* **9**, 15763 (2019). https://doi.org/10.1038/s41598-019-51904-4

[10] Lee, H., Huen, W.Y., Vimonsatit, V. et al. An Investigation of Nanomechanical Properties of Materials using Nanoindentation and Artificial Neural Network. Sci Rep 9, 13189 (2019). https://doi.org/10.1038/s41598-019-49780-z

[11] Le, Thinh-Tien, Johann Guilleminot, and Christian Soize. "Stochastic continuum modeling of random interphases from atomistic simulations. Application to a polymer nanocomposite." *Computer Methods in Applied Mechanics and Engineering* 303 (2016): 430-449.

[12] Bashirvand, S., and A. Montazeri. "FEM analysis of metal matrix nanocomposites reinforced with off-line atomistically-informed equivalent nanofillers." *Computational Materials Science* 129 (2017): 89-97.

[13] Liu, Y. J., et al. "A boundary element method for the analysis of CNT/polymer composites with a cohesive interface model based on molecular dynamics." *Engineering Analysis with Boundary Elements* 32.4 (2008): 299-308.

[14] Tran, A. T., Hung Le Quang, and Q-C. He. "Computation of the size-dependent elastic moduli of nano-fibrous and nano-porous composites by FFT." *Composites Science and Technology* 135 (2016): 159-171.

[15] Moulinec, Herve, and Pierre Suquet. "A fast numerical method for computing the linear and nonlinear mechanical properties of composites." *Comptes rendus de l'Académie des sciences*. Série II. Mécanique, physique, chimie, astronomie. (1994).

[16] Moulinec, Hervé, and Pierre Suquet. "A numerical method for computing the overall response of nonlinear composites with complex microstructure." *Computer methods in applied mechanics and engineering* 157.1-2 (1998): 69-94.

[17] Lee, S-B., R. A. Lebensohn, and Anthony D. Rollett. "Modeling the viscoplastic micromechanical response of two-phase materials using Fast Fourier Transforms." *International Journal of Plasticity* 27.5 (2011): 707-727.

[18] Monchiet, Vincent, and Guy Bonnet. "A polarization-based FFT iterative scheme for computing the effective properties of elastic composites with arbitrary contrast." *International Journal for Numerical Methods in Engineering* 89.11 (2012): 1419-1436.

[19] Willot, François, Bassam Abdallah, and Yves-Patrick Pellegrini. "Fourier-based schemes with modified Green operator for computing the electrical response of heterogeneous media with accurate local fields." *International Journal for Numerical Methods in Engineering* 98.7 (2014): 518-533.

[20] Nguyen, Trung-Kien, Karam Sab, and Guy Bonnet. "Green's operator for a periodic medium with traction-free boundary conditions and computation of the effective properties of thin plates." *International Journal of Solids and Structures* 45.25-26 (2008): 6518-6534.

[21] Salnikov, Vladimir, Daniel Choï, and Philippe Karamian-Surville. "On efficient and reliable stochastic generation of RVEs for analysis of composites within the framework of homogenization." *Computational Mechanics* 55.1 (2015): 127-144.

[22] Salnikov, Vladimir, et al. "Measure of combined effects of morphological parameters of inclusions within composite materials via stochastic homogenization to determine effective mechanical properties." *Composite Structures* 129 (2015): 122-131.

[23] Miller, Ronald E., and Vijay B. Shenoy. "Size-dependent elastic properties of nanosized structural elements." *Nanotechnology* 11.3 (2000): 139.

[24] Hashin, Zvi. "Thin interphase/imperfect interface in elasticity with application to coated fiber composites." *Journal of the Mechanics and Physics of Solids* 50.12 (2002): 2509-2537.

[25] Kiritsi, C. C., and N. K. Anifantis. "Load carrying characteristics of short fiber composites containing a heterogeneous interphase region." *Computational materials science* 20.1 (2001): 86-97.

[26] Duan, H. L., et al. "Size-dependent effective elastic constants of solids containing nano-inhomogeneities with interface stress." *Journal of the Mechanics and Physics of Solids* 53.7 (2005): 1574-1596.

[27] Dormieux, Luc, E. Lemarchand, and Sébastien Brisard. "Equivalent Inclusion Approach for Micromechanics Estimates of Nanocomposite Elastic Properties." *Journal of Nanomechanics and Micromechanics* 6.2 (2016): 04016002.

[28] Yvonnet, Julien, H. Le Quang, and Q-C. He. "An XFEM/level set approach to modelling surface/interface effects and to computing the size-dependent effective properties of nanocomposites." *Computational Mechanics* 42.1 (2008): 119-131.

[29] Michel, J. C., H. Moulinec, and Pierre Suquet. "A computational method based on augmented Lagrangians and fast Fourier transforms for composites with high contrast." *CMES(Computer Modelling in Engineering & Sciences)* 1.2 (2000): 79-88.

[30] Milton, G. W. The Theory of Composites. *Cambridge University Press*, 2002.

[31] Mori, Tanaka, and Kohichi Tanaka. "Average stress in matrix and average elastic energy of materials with misfitting inclusions." *Acta metallurgica* 21.5 (1973): 571-574.

[32] Kakavas, P.A., Anifantis, N.K., Baxevanakis, K. et al. The effect of interfacial imperfections on the micromechanical stress and strain distribution in fibre reinforced composites. *J Mater Sci* **30**, 4541–4548 (1995). https://doi.org/10.1007/BF01153060

[33] Wang, B., Fang, G., Liu, S. and Liang, J. Effect of heterogeneous interphase on the mechanical properties of unidirectional fiber composites studied by fft-based method. *Compos. Struct.* **220**, 642–651 (2019).